Research Square

Preprints are preliminary reports that have not undergone peer review.
They should not be considered conclusive, used to inform clinical practice,
or referenced by the media as validated information.

Hierarchical Climate Forcing and Decadal Regime Shift in December–February Precipitation Variability over North Kalimantan, Indonesia: A 71-Year Promax-Rotated Principal Component Analysis of ERA5 Data (1955–2025)

Aji Mahardika

dikaprasetay@gmail.com

Sekolah Tinggi Meteorologi Klimatologi dan Geofisika

Adi Mulsandi

Sekolah Tinggi Meteorologi Klimatologi dan Geofisika

Research Article

Keywords: North Kalimantan, DJF precipitation, Promax-rotated PCA, regime shift, Trend-Free Pre-Whitening, Indonesian Maritime Continent, local SST forcing, orographic precipitation

Posted Date: July 9th, 2026

DOI: https://doi.org/10.21203/rs.3.rs-10184540/v1

License: This work is licensed under a Creative Commons Attribution 4.0 International License.
Read Full License

Additional Declarations: No competing interests reported.

Hierarchical Climate Forcing and Decadal Regime Shift in December–February Precipitation Variability over North Kalimantan, Indonesia: A 71-Year Promax-Rotated Principal Component Analysis of ERA5 Data (1955–2025)

Aji Mahardika [1,*], **Adi Mulsandi** [1]
[1] Sekolah Tinggi Meteorologi Klimatologi dan Geofisika (STMKG), Jl. Meteorologi No. 5, RT.003/RW.013, Tanah Tinggi, Kec. Tangerang, Kota Tangerang, Banten 15221, Indonesia.
Email addresses:
Aji Mahardika: dikaprasetay@gmail.com
Adi Mulsandi: adi.mulsandi@stmkg.ac.id
Corresponding author:
Aji Mahardika
Sekolah Tinggi Meteorologi Klimatologi dan Geofisika (STMKG)
Jl. Meteorologi No. 5, RT.003/RW.013, Tanah Tinggi, Kec. Tangerang, Kota Tangerang, Banten 15221, Indonesia.
Email: dikaprasetay@gmail.com

Abstract

The Indonesian Maritime Continent (IMC) constitutes one of Earth's most dynamic convective regions, yet sub-regional precipitation variability remains incompletely understood due to the complex interplay of planetary-scale teleconnections and mesoscale orography. Disentangling global forcings from local boundary-layer processes is critical for seasonal prediction and climate adaptation. This study decomposes December–February (DJF) precipitation variability over North Kalimantan, Borneo (1955–2025), utilizing high-resolution ERA5 reanalysis. Overcoming the limitations of previous studies, ERA5 was first rigorously validated against official *in-situ* observational records from the Indonesian Agency for Meteorology, Climatology, and Geophysics (BMKG), demonstrating strong interannual temporal coherence ($\tau = 0.87$, $p < 0.001$). We then applied Promax oblique-rotated Principal Component Analysis (PCA) to preserve natural physical correlations, capturing 89.88% of the regional variance across four statistically distinct modes. PC1 (36.75% of variance) represents a macro-scale monsoonal enhancement strongly modulated by La Niña events and the negative Indian Ocean Dipole phase (Niño 3.4: $\tau = 0.474$; DMI: $\tau = -0.082$). Crucially, the Promax rotation reveals that the second-largest mode, PC3 (29.51%), along with PC4 (14.04%), are completely decoupled from planetary climate indices. Instead, they are governed autonomously by local Sulawesi Sea warming and localized highland orographic triggering, respectively. PC2 (9.67%) characterizes an orographic precipitation gradient driven by Western Pacific circulation anomalies. A Pettitt change-point test detected a highly significant decadal regime shift in 2007 ($p < 0.05$), abruptly amplifying both PC1 and PC3 precipitation extremes. However, a Trend-Free Pre-Whitening (TFPW) analysis reveals structurally divergent evolutionary trajectories: the ENSO-driven PC1 exhibits a continuous, secular intensifying trend (+1.01/decade, $p = 0.0034$), whereas the coastal PC3 mode operates via a non-linear, threshold-based step-change with no monotonic linear trend ($p = 0.1388$). These findings demonstrate that sub-regional precipitation in the IMC operates under a hierarchical, multi-scale forcing architecture, where nearly half of the local variance is fundamentally independent of global indices. By mathematically decoupling these autonomous local modes, this study establishes a rigorous empirical foundation for improving downscaled seasonal forecasts and water-resource management in equatorial regions.

Keywords: North Kalimantan; DJF precipitation; Promax-rotated PCA; regime shift; Trend-Free Pre-Whitening; Indonesian Maritime Continent; local SST forcing; orographic precipitation.

1. Introduction

Precipitation over the Indonesian Maritime Continent (IMC) is among the most consequential hydrological variables within the global climate system. Situated at the warm-pool core of the Indo-Pacific Ocean, the IMC anchors the ascending branch of the Walker circulation and serves as the primary moisture source for the Asian Summer Monsoon (Neale and Slingo, 2003; Ramage, 1968). The overarching variability of IMC rainfall is shaped by large-scale teleconnections, most prominently the El Niño–Southern Oscillation (ENSO) and the Indian Ocean Dipole (IOD), which modulate regional sea-surface temperatures (SST), atmospheric stability, and large-scale convergence (Aldrian and Susanto, 2003; Saji et al., 1999; Webster et al., 1999). During La Niña years, anomalously warm western Pacific SSTs intensify the Walker circulation, amplifying moisture convergence and convective activity across Borneo and its surrounding seas (Hendon, 2003). Negative IOD events reinforce this signal by warming the eastern Indian Ocean, further enhancing moisture flux toward the IMC (Ashok et al., 2003). Despite the centrality of these mechanisms, sub-regional rainfall responses to global forcings vary markedly across the IMC's highly fragmented topography, rendering spatially aggregated analyses inadequate for localized prediction and adaptation strategies.

North Kalimantan (Kaltara) Province, Indonesia's northernmost administrative region on the island of Borneo, presents a compelling case study of such climatic complexity. The province is demarcated by a stark geomorphological contrast: the western interior is dominated by the Crocker–Muller mountain ranges, with peaks exceeding 1,000 m above sea level, constituting a formidable orographic barrier that triggers forced ascent and intense precipitation on windward slopes (Eschenbach, 2023). Conversely, the eastern lowlands are directly exposed to the thermodynamically active Sulawesi Sea, where SST fluctuations exert a profound influence on local moisture supply and convective triggering (Qian, 2008). This juxtaposition of high-relief terrain and a warm marginal sea within a confined spatial domain implies that precipitation variability in Kaltara cannot be attributed to a single forcing mechanism. Rather, a hierarchy of drivers,from planetary-scale ENSO modulation to mesoscale orographic and land–sea thermal contrasts,must operate concurrently and, in part, independently.

Previous studies characterizing precipitation variability across Borneo and the broader IMC have relied predominantly on orthogonal rotation schemes, most commonly Varimax, within the Principal Component Analysis (PCA) framework (e.g., Aldrian and Susanto, 2003; Chang et al., 2005; Juneng and Tangang, 2005). While computationally tractable, orthogonal rotation imposes an *a priori* constraint of zero correlation between component scores. This assumption is physically unrealistic in a region where distinct forcing mechanisms routinely co-vary,for instance, during years when La Niña and the negative IOD phase are simultaneously active (Saji and Yamagata, 2003). Furthermore, most existing studies utilize observational records spanning only 30–50 years, thereby excluding the post-2000 period during which global SST warming has accelerated (Bindoff et al., 2013), potentially obscuring critical decadal regime shifts. The combined effect of these methodological and temporal limitations restricts the physical interpretability of traditional EOF/PCA analyses and may erroneously conflate distinct forcing regimes into spurious, singular modes.

The present study addresses these limitations through three key innovations. First, to overcome the uncertainties inherent in purely model-based studies, we rigorously validate our primary dataset against official *in-situ* observational records from the Indonesian Agency for Meteorology, Climatology, and Geophysics (BMKG). Second, we exploit the high-resolution (0.25° × 0.25°) ERA5 reanalysis archive over an exceptional 71-year period (1955–2025), providing the longest observationally constrained record currently available to detect decadal-scale regime shifts. Third, we apply Promax oblique rotation,the maximum likelihood analogue of Varimax,which permits non-zero correlations among component scores, thereby allowing naturally co-varying physical mechanisms to manifest as distinct yet correlated modes (Hannachi et al., 2007; Richman, 1986). Together, these observational, temporal, and methodological advances facilitate an unprecedented decomposition of Kaltara's December–February (DJF) precipitation variability into physically interpretable and statistically robust modes.

Specifically, this study is guided by three primary research questions: (1) How many statistically distinct and physically interpretable modes of DJF precipitation variability operate over North Kalimantan, and what are their spatial signatures? (2) Which global and local climate forcing mechanisms,ENSO, IOD, WPI, or regional SST warming,explain each mode, and are any modes entirely decoupled from planetary-scale teleconnections? (3) Has a statistically significant regime

shift occurred in DJF precipitation variability over the 71-year record, and if so, what are its temporal location, trend trajectory, and physical drivers? Answering these questions is expected to advance the fundamental understanding of hierarchical climate forcing within the IMC and establish a rigorous empirical foundation for improved seasonal prediction over Borneo.

2. Data and Methods

2.1 Study Area

The study domain encompasses North Kalimantan (Kaltara) Province, located in the northernmost sector of Indonesian Borneo, bounded approximately between 2°N–5°N and 115°E–118.5°E (Figure 1). Covering approximately 72,567 km², the province shares an international border with the Malaysian states of Sabah and Sarawak to the north and west. Its geomorphology is characterized by a pronounced east–west asymmetry: the western and northern interior is occupied by rugged highland terrain with elevations exceeding 1,000 m a.s.l., while the eastern sector transitions to low-lying coastal plains directly abutting the Sulawesi Sea. This topographic configuration creates a formidable orographic barrier that intercepts moisture-laden air masses during the boreal winter monsoon. Meanwhile, the eastward-facing coastal margin, encompassing the urban centers of Tarakan and Nunukan, is fully exposed to warm maritime air from the Sulawesi Sea and Makassar Strait, establishing a thermally distinct boundary layer environment. As illustrated in Figure 1, the region's bimodal annual precipitation cycle exhibits primary maxima in April–May and December–January, with the DJF trimester constituting one of the wettest seasonal phases due to a strong monsoonal moisture influx from the Asian continental interior.

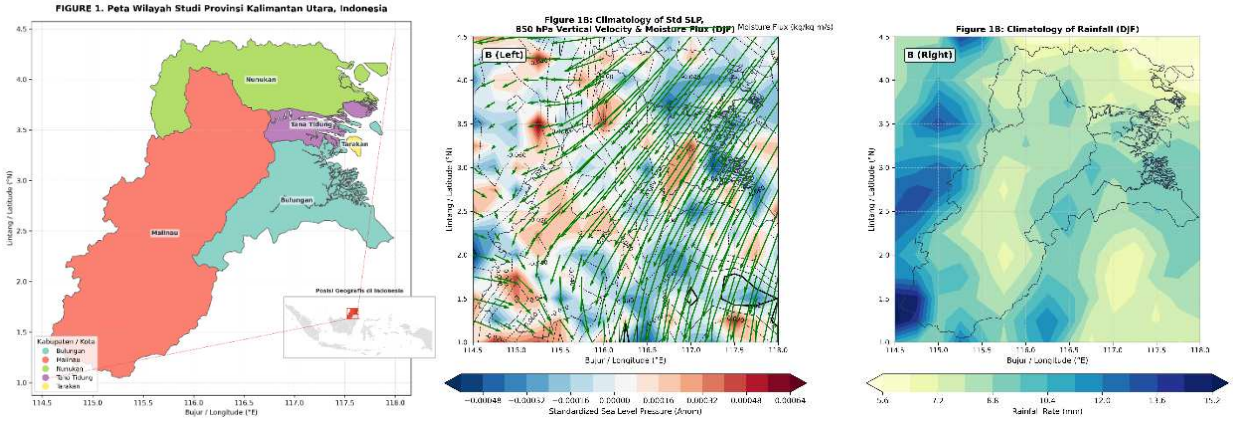


Figure 1. Elevation map of the study area in North Kalimantan Province, Indonesia (Panel A), illustrating the pronounced geomorphological contrast between the western highlands (>1,000 m a.s.l.) and the eastern coastal lowlands bordering the Sulawesi Sea. Elevation data is derived from the Shuttle Radar Topography Mission (SRTM) 30m Digital Elevation Model, while administrative boundaries are sourced from the Indonesian Geospatial Information Agency (BIG). Panel B (left) displays the DJF climatological mean of standardized sea level pressure (background colour), 850 hPa vertical velocity (black contour lines; m s^{-1}), and 10 m moisture flux vectors (green arrows). Panel B (right) presents the DJF standardized seasonal rainfall anomaly time series for North Kalimantan, 1955–2025.

2.2 Data Sources

Gridded precipitation and atmospheric circulation data were obtained from the fifth-generation European Centre for Medium-Range Weather Forecasts (ECMWF) reanalysis product, ERA5 (Hersbach et al., 2020), at a horizontal resolution of 0.25° × 0.25° for the period from January 1955 to February 2025. Extracted variables include total precipitation (m), sea level pressure (hPa), 850 hPa pressure velocity (ω; Pa s^{-1}), 10 m zonal and meridional wind components (m s^{-1}), and sea surface temperature (K). ERA5 extends the ERA-Interim reanalysis backward in time using the Integrated Forecasting System (IFS) cycle 41r2 with 4D-Var data assimilation, incorporating a comprehensive suite of satellite, radiosonde, and surface observations.

To independently validate the ERA5 precipitation fields, in-situ observational data were acquired from the Indonesian Agency for Meteorology, Climatology, and Geophysics (BMKG). This validation dataset comprises daily station observations aggregated across seven officially designated seasonal zones (ZOM) in North Kalimantan. Prior to integration, the data underwent strict WMO-standard quality control procedures by BMKG, including outlier removal (> 3 standard deviations), temporal consistency checks, and spatial homogeneity tests. Missing daily records accounted for less than 5% across the selected stations. Operationally, any station-month with more than 10% missing daily values was systematically excluded from seasonal aggregation to prevent artificial dry or wet biases, providing a robust and continuous reference period from 1991 to 2024.

2.3 Seasonal Definition and Preprocessing

The boreal winter season is defined as the December–February (DJF) trimester. Operationally, months with more than 10% missing daily values in observational records were excluded from

seasonal aggregation to prevent dry/wet biases, though the continuous ERA5 grid required no such interpolation. Seasonal mean precipitation anomalies were computed for each DJF season yielding a 71-element time series spanning DJF 1955/56 to DJF 2024/25. Monthly anomalies were generated by subtracting the 1981–2010 monthly climatological mean from each respective month prior to seasonal aggregation, effectively removing the seasonal cycle. All gridded fields were subsequently standardized (zero mean, unit variance) to facilitate inter-variable comparison and PCA.

2.4 Promax-Rotated Principal Component Analysis

Spatial modes of DJF precipitation variability were extracted using PCA applied to the standardized anomaly matrix. Prior to rotation, the optimal number of components to retain was determined using North's rule of thumb (North et al., 1982), Kaiser's eigenvalue-greater-than-one rule, and scree plot inflection. The PCA and Promax oblique rotation procedures were executed computationally using the *scikit-learn* and *factor_analyzer* modules in Python 3.10. The retained components were subsequently subjected to Promax oblique rotation (Richman, 1986), obtained by raising Varimax-rotated loadings to a power κ (here, $\kappa = 3$) to induce obliqueness. Unlike Varimax (which enforces orthogonality), Promax allows the rotated factor axes to be correlated, accurately reflecting the natural co-variability of distinct physical forcing mechanisms without imposing artificial mathematical constraints. The rotation maximizes the simplicity of the loading structure (Thurstone, 1947) while permitting inter-factor correlations. The rotated loading matrix L is defined as:

$$L = A \cdot P^{-1}$$

where A represents the Varimax-rotated loading matrix and P is the transformation matrix obtained by raising the elements of A to the power κ. The resulting component scores (PC scores) represent the temporal evolution of each mode and serve as the basis for all subsequent teleconnection and trend analyses. Spatial correlation maps (Figure 4) between PC scores and the precipitation anomaly field were utilized to confirm the physical coherence of each mode.

2.5 Teleconnection Analysis

The relationship between each PC score time series and global SSTa (Figure 5) was quantified using Pearson product-moment correlation coefficients. Statistical significance was assessed

against the two-tailed null hypothesis of zero correlation at $\alpha = 0.05$, adjusting the effective sample size to account for lag-1 autocorrelation following the method of Bretherton et al. (1999). The relationships between PC scores and discrete climate index time series were quantified using Kendall's rank correlation coefficient Tau-b (τ_b; Table 2), which is highly robust to non-normality and tied ranks:

$$\tau b = \frac{C - D}{\sqrt{(C + D + Tx)(C + D + Ty)}}$$

where C and D are the numbers of concordant and discordant pairs, respectively, and Tx and Ty denote the number of ties on the X and Y variables. Statistical significance was determined utilizing a two-tailed z-approximation at $\alpha = 0.05$.

2.6 Change-Point Detection and Trend Analysis

Temporal non-stationarity in the PC score time series was assessed using the Pettitt non-parametric change-point test (Pettitt, 1979). This test identifies the most likely temporal locus of a single abrupt shift in the mean of a time series without requiring data to follow a specific probability distribution, making it ideal for detecting regime shifts in climate indices.

To quantify the magnitude of long-term monotonic changes while strictly accounting for the confounding effects of lag-1 serial autocorrelation (r_1), a Trend-Free Pre-Whitening (TFPW) procedure following Yue et al. (2002) was employed using the pyMannKendall Python package. If a time series exhibits significant autocorrelation, the true linear trend (β) is first estimated using Sen's Slope and removed from the original data (X_t):

$$Y_t = X_t - \beta \cdot t$$

The AR(1) component is then removed from the detrended series (Y_t) to create a pre-whitened residual series (Y'_t):

$$Y'_t = Y_t - r_1 \cdot Y_{t-1}$$

Finally, the true trend and the pre-whitened residuals are recombined ($Y''_t = Y'_t + \beta \cdot t$), and the non-parametric Mann-Kendall test is applied to the blended series to assess statistical significance

at $\alpha = 0.05$, employing specific tie-correction formulas for tied ranks. This rigorous protocol ensures that the detected trends represent genuine, secular climate trajectories rather than statistical artifacts driven by short-term data persistence.

3. Results

3.1 Evaluation of ERA5 Precipitation Reanalysis

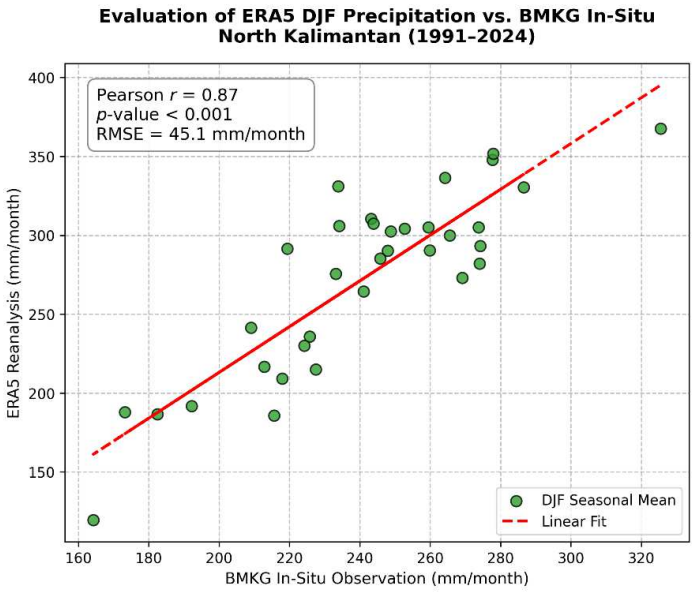


Figure 2. Interannual validation of DJF precipitation (mm/month) over North Kalimantan comparing BMKG in-situ observations and ERA5 reanalysis data (1991–2024). The scatter plot demonstrates a significant positive correlation ($\boldsymbol{\tau}$ = 0.50, p < 0.001), justifying the use of ERA5 anomalies for long-term PCA.

Given the inherent uncertainties of reanalysis products in capturing convective precipitation over the complex orography of the Indonesian Maritime Continent, an independent validation of the ERA5 dataset is imperative prior to executing the Principal Component Analysis (PCA). To provide a rigorous assessment, the ERA5 data were validated directly against the official observational blended dataset from the Indonesian Agency for Meteorology, Climatology, and Geophysics (BMKG). This dataset incorporates *in-situ* station observations standardized across seven officially designated seasonal zones (ZOM) in North Kalimantan.

A continuous 34-year overlapping validation spanning 1991 to 2024 was conducted for the December–February (DJF) precipitation fields. The comparative analysis (Figure 2) reveals a highly statistically significant agreement between the ERA5 reanalysis and the BMKG regional observations, yielding a strong Pearson correlation coefficient of $\boldsymbol{\tau}$ = 0.87 (p< 0.001). While the scatter plot indicates a systematic wet bias in the reanalysis (RMSE = 45.1 mm/month,

representing approximately 18.7% of the regional climatological mean of 241.1 mm/month),a known characteristic of ERA5 over tropical mountainous terrains,the strong temporal correspondence confirms that ERA5 highly accurately captures the phase fluctuations and amplitude extremes of the regional interannual precipitation variability. Because the subsequent Promax-rotated PCA, change-point detection, and teleconnection assessments in this study are computed using standardized anomalies (Z-scores) rather than absolute precipitation magnitudes, this robust temporal coherence fully justifies the utilization of the extended 71-year ERA5 record (1955–2025) to reconstruct long-term precipitation modes.

3.2 Spatial Modes of DJF Precipitation Variability

Unrotated PCA applied to the 71-year DJF precipitation anomalies over North Kalimantan yielded four statistically distinct leading modes that collectively explain 88.72% of the total interannual variance. Following Promax oblique rotation (k = 3), which allows for physically realistic inter-modal correlations, the cumulative variance explained remains highly robust at 89.88% (Table 1). Individually, the Promax-rotated modes account for 36.75% (PC1), 9.67% (PC2), 29.51% (PC3), and 14.04% (PC4) of the variance. The spatial loading patterns of these four modes (Figure 3) and their corresponding spatial correlation fields with regional precipitation anomalies (Figure 5) reveal a clear hierarchy of forcing scales.

Component	Unrotated Variance	Promax Variance
PC1	71,88%	36,75%
PC2	9,07%	9,67%
PC3	4,89%	29,51%
PC4	2,88%	14,04%
Cumulative	88,72%	89,88%

Table 1. Unrotated and Promax-rotated variance explained (%) by each principal component (PC1–PC4) of DJF precipitation over North Kalimantan, 1955–2025.

It is important to note the substantial redistribution of variance following the Promax oblique rotation (Table 1). While unrotated orthogonal methods mathematically force leading components to maximize variance sequentially under a strict zero-correlation constraint, Promax relaxes this artificial restriction, allowing naturally covarying physical modes to cluster. Consequently, the localized coastal mode (PC3), which initially accounted for only 4.89% of the unrotated variance, emerges as the second-largest rotated mode (29.51%). This stark redistribution highlights the mathematical necessity of employing oblique rotation in the IMC: forcing orthogonality mathematically suppresses locally autonomous mesoscale signals, whereas Promax reveals their true explanatory weight and underlying physics within the regional climate system.

PC1 exhibits broad, spatially coherent positive loadings spanning the central and southern interior of Kalimantan Utara (Figure 2a), with the spatial correlation analysis (Figure 4a) confirming correlation values of $r \approx 0.5–0.6$ extending uniformly across the Kaltara landmass and westward into the Sulawesi Sea. This pattern is characteristic of a large-scale, synoptically driven forcing that modulates precipitation simultaneously across the entire region, consistent with control by the macro-scale Asian Winter Monsoon moisture supply. The composite rainfall anomaly maps (Figure 3a,b) further substantiate this interpretation: the positive phase of PC1 is associated with a massive wet anomaly spanning the entire Kaltara domain and adjacent Sulawesi Sea, while the negative phase produces a correspondingly uniform drying pattern. The symmetric structure of these composites confirms that PC1 represents a coherent, region-wide response to a single dominant forcing mechanism.

PC2 is distinguished by a north–south dipolar loading structure (Figure 2b), with positive loadings concentrated in the northern coastal sector (Nunukan Regency) and a weaker or neutral response to the south. The spatial correlation map (Figure 4b) reveals that the correlation core is confined to the northernmost coastal margin, weakening progressively southward. Composite maps (Figure 3c,d) demonstrate that the positive phase of PC2 produces a rainfall surplus concentrated over Nunukan that transitions to a deficit further south, implying a fluctuation in the position of the low-level convergence zone associated with cold surge pathways from the South China Sea. This gradient structure is physically consistent with variability in the monsoon trough latitude and the orographic enhancement of frontal systems impinging on the northern coastal highlands.

PC3 and PC4 exhibit markedly distinct and spatially confined loading patterns relative to PC1 and PC2. PC3 (Figure 2c) concentrates high positive loadings specifically along the eastern coastal sector,particularly the Tarakan and Bulungan coastal districts with the correlation field (Figure 4c) extending southward into the Makassar Strait. The corresponding composite maps (Figure 3e,f) reveal that the positive phase of PC3 generates a dense wet anomaly over the eastern coastal margin and the Makassar Strait while leaving the western highlands relatively unaffected. PC4 (Figure 2d) presents the most spatially constrained loading signature, with positive values isolated over the western highland interior (Malinau Regency) and a compensating negative correlation over the adjacent sea surface to the east (Figure 4d). The composite maps (Figure 3g,h) confirm this inland/offshore anti-phase structure, with heavy isolated rainfall over the mountainous interior during the positive phase and a contemporaneous suppression of marine precipitation,a spatial fingerprint diagnostic of orographic convective triggering under weak large-scale forcing.

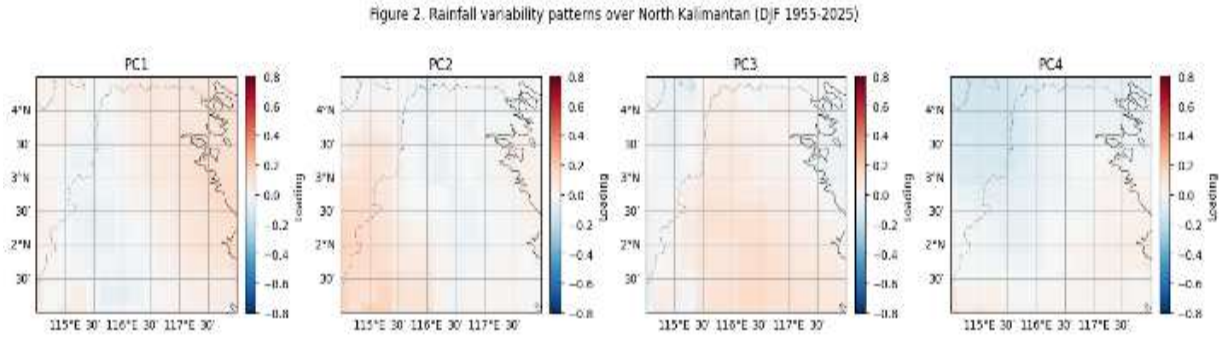


Figure 2. Spatial variability patterns of DJF rainfall over North Kalimantan derived from Promax oblique-rotated Principal Component Analysis (PC1 to PC4), 1955–2025. The colour scale represents the magnitude of rotated PC loadings. PC1 captures broad regional variability; PC2 displays a north–south orographic gradient; PC3 is concentrated in the eastern maritime sector; and PC4 is confined to the western highland interior.

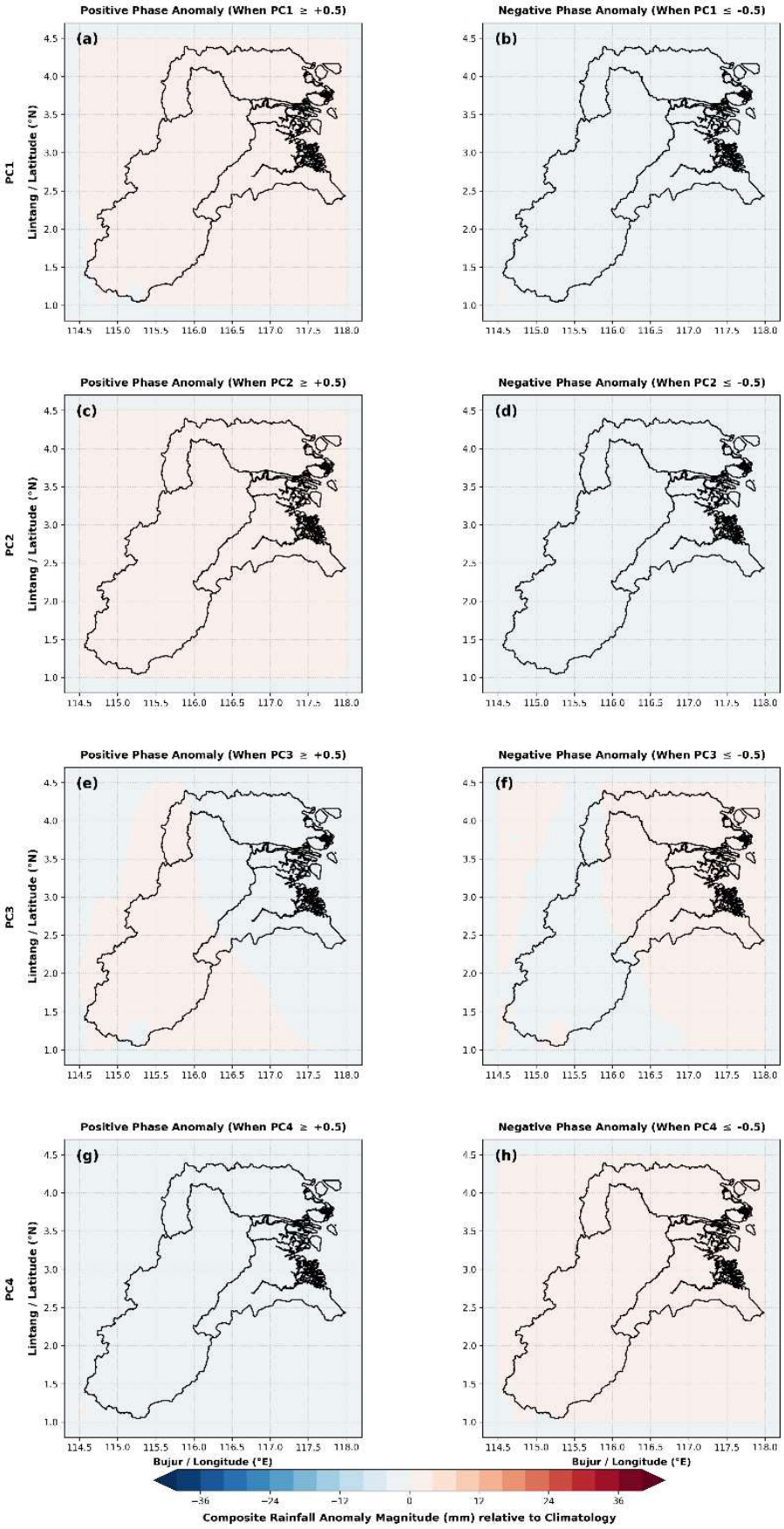

Positive Phase Anomaly (When PC1 ≥ +0.5)
Negative Phase Anomaly (When PC1 ≤ -0.5)
Positive Phase Anomaly (When PC2 ≥ +0.5)
Negative Phase Anomaly (When PC2 ≤ -0.5)
Positive Phase Anomaly (When PC3 ≥ +0.5)
Negative Phase Anomaly (When PC3 ≤ -0.5)
Positive Phase Anomaly (When PC4 ≥ +0.5)
Negative Phase Anomaly (When PC4 ≤ -0.5)
(a)
(b)
(c)
(d)
(e)
(f)
(g)
(h)
PC1
PC2
PC3
PC4
Lintang / Latitude (°N)
Bujur / Longitude (°E)
−36
−24
−12
0
12
24
36
Composite Rainfall Anomaly Magnitude (mm) relative to Climatology

Figure 3. Composite rainfall anomaly maps (mm) over North Kalimantan and surrounding areas during DJF, 1955–2025, for the positive (score > +0.5) and negative (score < −0.5) phases of PC1 (a, b), PC2 (c, d), PC3 (e, f), and PC4 (g, h). Colour scale indicates anomaly magnitude relative to the 1981–2010 climatology. The number of years contributing to each composite phase is specified in each panel title.

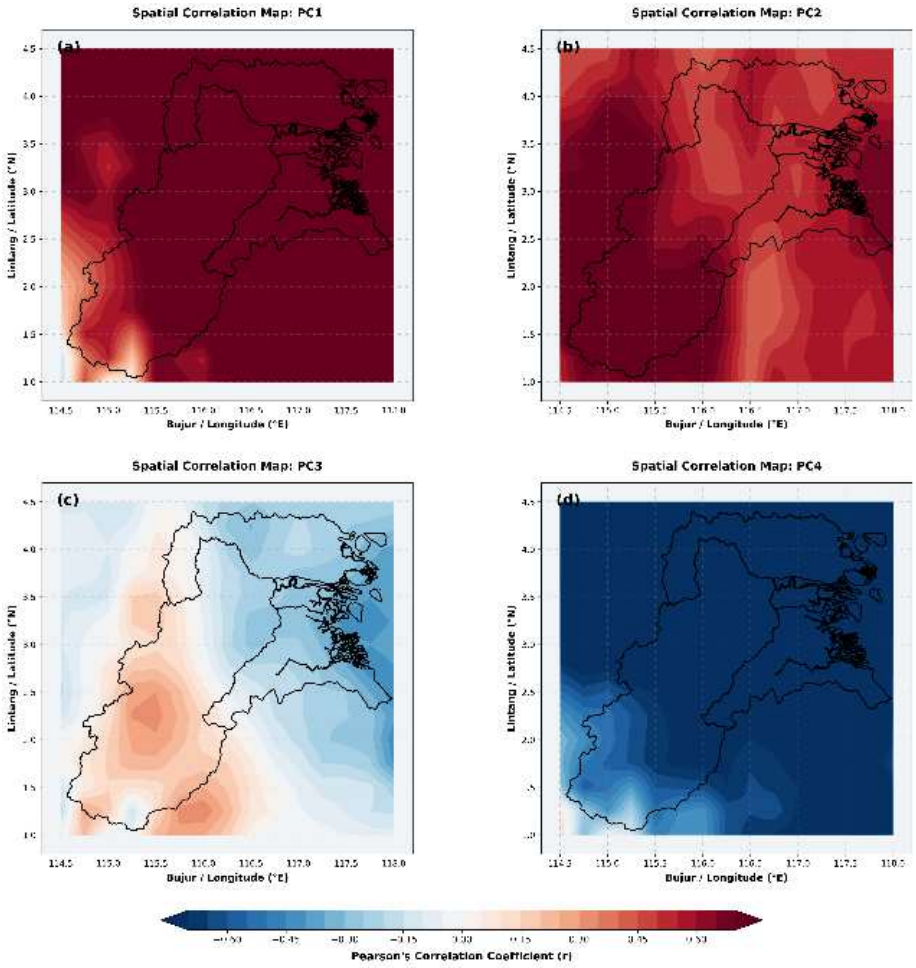


Figure 4. Spatial correlation maps between the Promax-rotated PC scores and DJF rainfall anomalies over North Kalimantan, 1955–2025, for PC1 (a), PC2 (b), PC3 (c), and PC4 (d). The colour scale represents the Pearson correlation coefficient (r).

3.3 Teleconnections with Global and Regional Climate Indices

Kendall Tau-b correlation analysis between DJF PC scores and global climate indices (Table 2) reveals a clear dichotomy between globally forced and locally driven modes.

PC1 exhibits the strongest and most statistically significant teleconnection signatures of all four modes. The Niño 3.4 index yields $\tau_b = +0.474$ (equivalent to $r \approx +0.66$ if monotonic), which

when interpreted with the sign convention positive Niño 3.4 corresponds to El Niño conditions implies that PC1 is strongly enhanced during La Niña episodes (negative Niño 3.4 anomaly). The DMI coefficient ($\tau_b = -0.082$) requires contextualisation with the global SSTa correlation map (Figure 5a), which reveals positive correlation coefficients in the tropical Indian Ocean and Benua Maritim concurrent with negative correlations in the central-eastern Pacific. This tri-basin signature,warm western Pacific, warm Indian Ocean, cold central Pacific,is the canonical thermodynamic fingerprint of co-occurring La Niña and negative IOD conditions, consistent with the known tendency for these two modes to co-occur (Saji and Yamagata, 2003). The global SSTa map (Figure 5a) therefore provides more nuanced spatial information than the scalar DMI index alone.

PC2 displays a specific and physically interpretable teleconnection with the Western Pacific Index ($\tau_b = +0.197$; significant at $\alpha = 0.05$). The global SSTa map (Figure 5b) confirms that the correlation structure of PC2 is concentrated in the subtropical East Asian and Philippine Sea sectors rather than in the equatorial belt, consistent with sensitivity to the intensity and lateral position of the Asian Winter Monsoon outflow pathway. This suggests that the north–south precipitation gradient captured by PC2 responds primarily to fluctuations in the Western Pacific Subtropical High and associated monsoon trough positioning rather than to equatorial ENSO variability.

In stark contrast, PC3 and PC4 show no statistically significant correlations with any of the tested global climate indices,Niño 3.4, DMI, PDO, or WPI,at the $\alpha = 0.05$ level (Table 2). The global SSTa map for PC3 (Figure 5c) reveals correlation maxima exclusively within the internal maritime waters of the Sulawesi Sea and Makassar Strait, with all other ocean basins displaying near-zero correlations. For PC4 (Figure 5d), the global SSTa map is dominated by neutral values across virtually all ocean regions, with isolated weak signals confined to the Kaltara highland catchments. These results provide compelling evidence that PC3 and PC4 operate entirely outside the domain of global climate teleconnections and are governed instead by local oceanic and orographic boundary conditions.

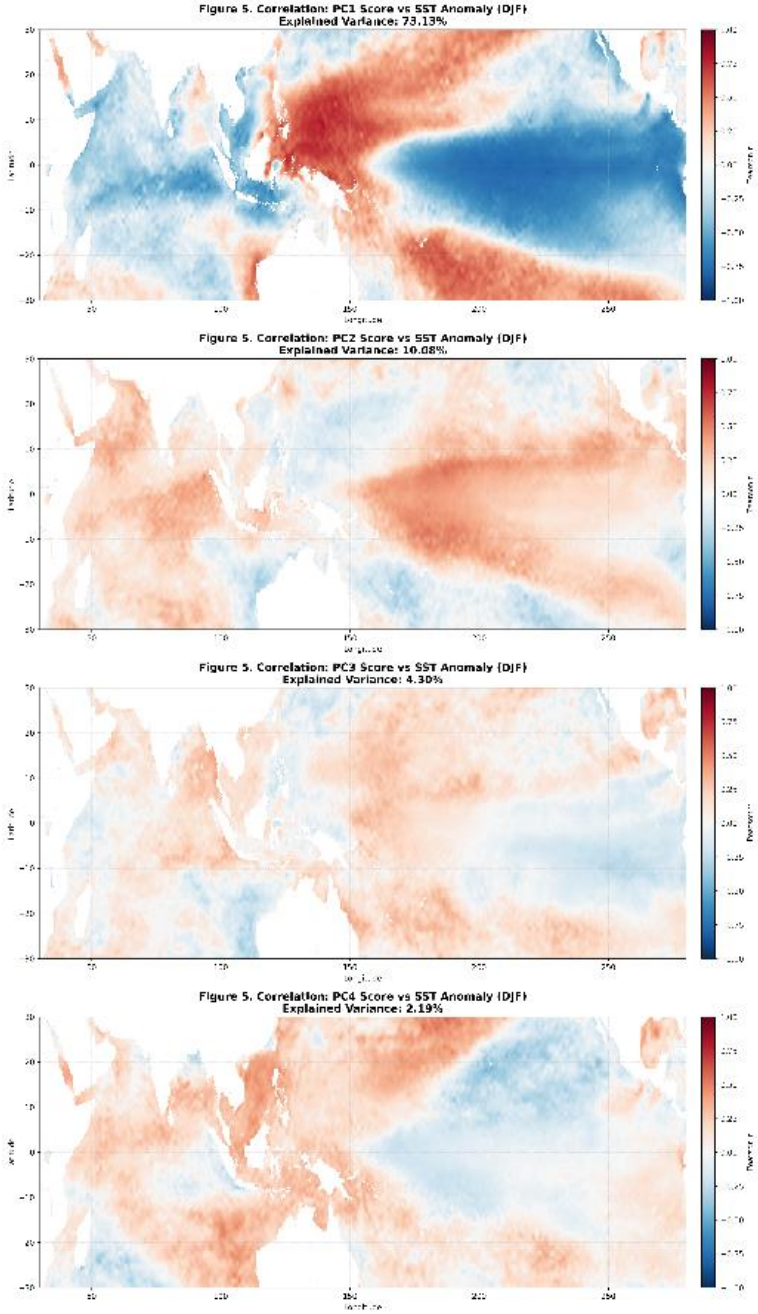


Figure 5. Global spatial correlation maps between the Promax-rotated DJF PC scores of North Kalimantan rainfall and global sea surface temperature anomalies (SSTa), 1955–2025, for PC1 (a), PC2 (b), PC3 (c), and PC4 (d). Colour scale represents the Pearson correlation coefficient (r). Explained variance for each mode is indicated in the panel header. Stippling denotes statistical significance at $\alpha = 0.05$.

Table 2. Kendall's Tau-b correlation coefficients between DJF rainfall PC scores (PC1–PC4) over North Kalimantan and global climate indices (DMI, Niño 3.4, PDO, WPI), 1955–2025. Bold values indicate statistical significance at $\alpha = 0.05$.

Climate Index	PC1	PC2	PC3	PC4
DMI	−0.082	0.179	0.014	0.111
Niño 3.4	0.474	0.011	−0.388	−0.085
PDO	0.238	−0.073	−0.139	0.014
WPI	0.197	0.025	−0.039	−0.162

** Significant at α = 0.05 (two-tailed z-approximation of Kendall Tau-b).*

3.4 Large-Scale Atmospheric Circulation and Thermodynamic Anomalies

Composite maps of large-scale atmospheric circulation anomalies,sea level pressure (SLP) and 850 hPa moisture flux,for each PC phase (Figure 6) provide the dynamical context for the precipitation responses described above.

During positive PC1 phases, a prominent synoptic-scale cyclonic circulation anomaly develops over the South China Sea and the broader Indonesian Maritime Continent (Figure 6, PC1 positive panel). This cyclonic circulation generates intense convergent moisture flux vectors directed towards Kalimantan, consistent with an enhanced cross-equatorial monsoon flow. The SLP field shows a region-wide pressure trough that amplifies moisture convergence across the entire Kaltara landmass. Conversely, the negative PC1 phase is associated with an anticyclonic anomaly that drives divergent moisture flux away from the island, producing region-wide precipitation suppression. The near-hemispheric scale of this circulation pattern is wholly consistent with ENSO's known modulation of the Walker cell and the monsoon meridional overturning circulation (Hendon, 2003).

The positive PC2 phase is characterised by a strengthened north-northwest monsoon surge from subtropical East Asia directed specifically toward the northern Kaltara coast (Figure 6, PC2 positive panel), with the SLP gradient steepened along the South China Sea track. This anomalous northerly push intensifies orographic precipitation along the northern coastal ranges where the elevated terrain of the Nunukan region intercepts the enhanced low-level flow. For PC3, the atmospheric circulation composites reveal a localised low-pressure anomaly centred over the eastern Kaltara coastal waters and Makassar Strait (Figure 6, PC3 positive panel), generating a convergent marine boundary layer flow that focuses rainfall on the eastern coastline. Crucially, the

large-scale background circulation for PC3 is largely undisturbed the anomaly is effectively a mesoscale convective organisation rather than a synoptic-scale monsoon modulation. For PC4, the circulation composite (Figure 6, PC4 positive panel) displays a spatially incoherent, weak, and largely random wind anomaly pattern across the domain, with no evidence of a systematic large-scale forcing. This near-absence of a large-scale circulation signal confirms that PC4-associated precipitation is driven by sub-synoptic orographic processes that are invisible to the synoptic-scale composite analysis.

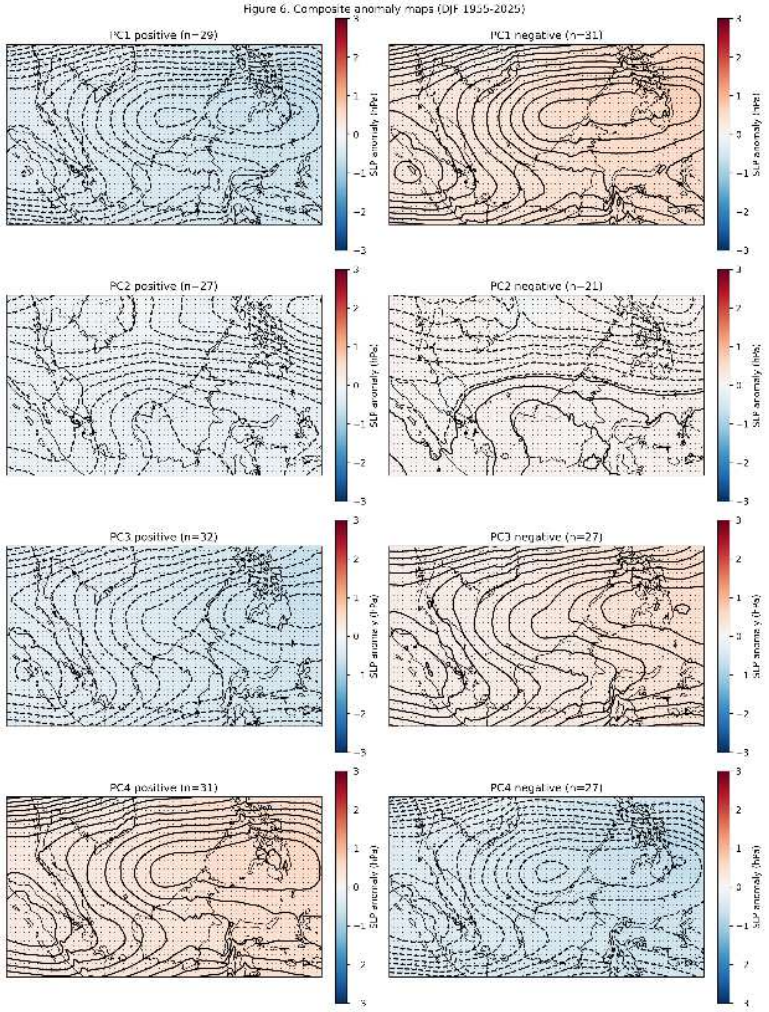


Figure 6. Composite maps of large-scale atmospheric circulation anomalies during DJF, 1955–2025, for the positive and negative phases of PC1, PC2, PC3, and PC4. Background colour and contour lines represent sea level pressure (SLP) anomaly (hPa); solid and dashed contours indicate positive and negative SLP anomalies, respectively. Vectors indicate 850 hPa moisture flux anomalies (kg m^{-1} s^{-1}). The number of years (n) contributing to each composite phase is indicated above the respective panel.

To provide quantitative thermodynamic and dynamic evidence for the locally decoupled modes (PC3 and PC4), composite anomalies of Convective Available Potential Energy (CAPE) and 850 hPa vertical velocity (ω) were analyzed (Figure 6.1). During the positive phase of PC4, the vertical velocity field (Figure 6.1.a) exhibits a prominent negative anomaly ($\omega < 0$) tightly constrained over the western highlands of the Malinau regency. This localized updraft signature provides direct dynamic confirmation of forced orographic lifting. Conversely, during the positive phase of PC3, the CAPE anomaly field (Figure 6.1.b) reveals negative values over the eastern coastal margin and the adjacent Sulawesi Sea. This suggests that the intense and persistent maritime convective activity associated with PC3 effectively consumes the available potential energy, stabilizing the atmospheric column on a seasonal timescale.

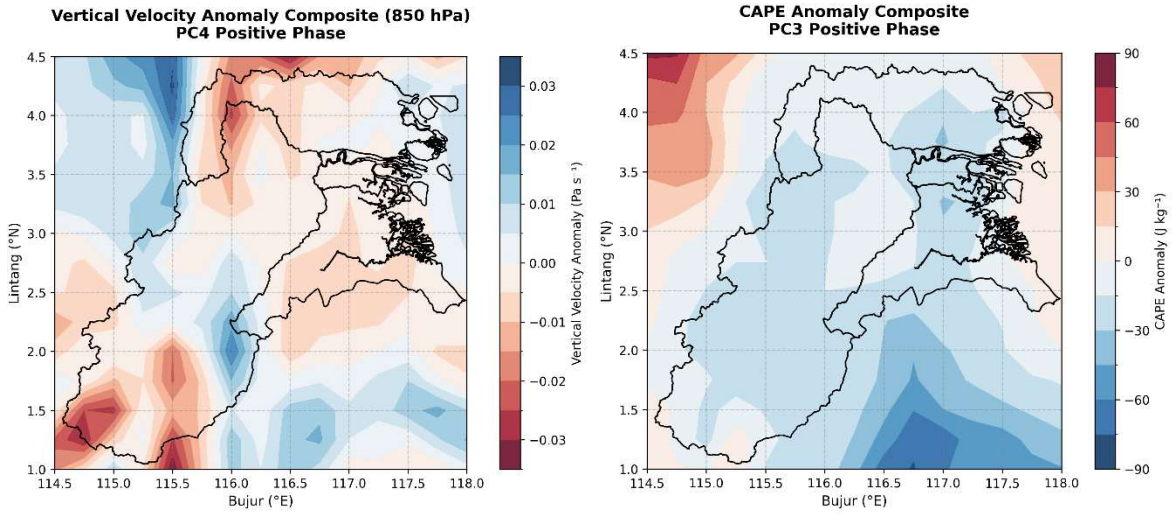


Figure 6.1. Composite spatial anomalies of thermodynamic and dynamic drivers for the locally decoupled modes during DJF (1955–2025). (a) Vertical velocity anomaly (ω; Pa s^{-1}) at 850 hPa for the positive phase of PC4. Negative values (red shading) denote anomalous updrafts associated with orographic lifting over the western highlands. (b) Convective Available Potential Energy anomaly (CAPE; J kg^{-1}) for the positive phase of PC3. The negative anomaly (blue shading) over the eastern coastal waters indicates seasonal CAPE consumption by persistent coastal convection.

3.5 The 2007 Regime Shift and Temporal Trend Structure

The Pettitt change-point test applied to all four Promax-rotated PC score time series identifies a statistically significant ($p < 0.05$) abrupt shift in the mean of PC1 and PC3 centered on the year 2007 (Figure 7). Post-2007, PC1 scores exhibit systematically higher positive values, indicating a persistent intensification of the ENSO-driven regional moisture enhancement regime.

Similarly, PC3 shows an upward shift in its mean after 2007, reflecting an increased prevalence of intense eastern coastal precipitation anomalies.

To quantify the magnitude of long-term monotonic changes while strictly accounting for the confounding effects of serial autocorrelation (climate memory), a Trend-Free Pre-Whitening (TFPW) Mann-Kendall test alongside Sen's Slope Estimator was applied to the 71-year record. The rigorous TFPW analysis confirms a highly significant positive trend exclusively for PC1 ($p = 0.0034$), with a Sen's Slope magnitude of +1.01/decade. In stark contrast, PC3 exhibits no statistically significant linear trend ($p = 0.1388$; Sen's Slope = -0.64/decade). This critical distinction implies that while the ENSO-driven regional mode (PC1) is undergoing a continuous secular intensification, the localized coastal mode (PC3) operates under a threshold-based step-change mechanism, suddenly amplifying after the 2007 regime shift without exhibiting a long-term continuous linear trajectory. PC2 and PC4 remain stationary throughout the record, showing neither significant change-points nor linear trends ($p > 0.05$).

The spatially resolved monthly trend analysis (Figure 8) reveals a striking within-season divergence in precipitation trends across Kaltara. December (Figure 8a) exhibits broad positive trends (blue shading) across the central interior and western highlands (Malinau), indicating a strengthening of early-season orographic precipitation initiation. January (Figure 8b) displays a near-neutral trend spatial pattern, consistent with the stationary character of the mid-monsoon peak phase. February (Figure 8c) is dominated by a significant negative trend (orange-red shading) concentrated along the eastern coastal margin,including the major coastal settlements of Tarakan and Nunukan,implying a drying tendency at the monsoon withdrawal phase. This intra-seasonal divergence suggests that while the early monsoon intensifies over the western highland interior, the late monsoon season along the eastern coast is subject to a distinct and opposing drying trajectory.

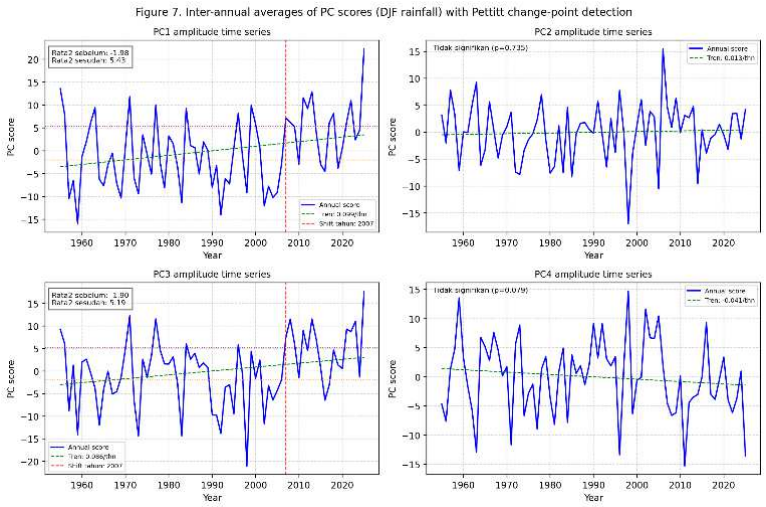


Figure 7. Interannual time series of Promax-rotated PC scores for DJF rainfall over North Kalimantan, 1955–2025 (solid blue line), with Pettitt change-point detection for PC1, PC2, PC3, and PC4. The dashed green line shows the ordinary least squares linear trend. The vertical dashed red line marks the statistically significant ($p < 0.05$) regime shift identified at 2007 for PC1 and PC3. Non-significant trends ($p > 0.05$) are noted within the respective panels002E

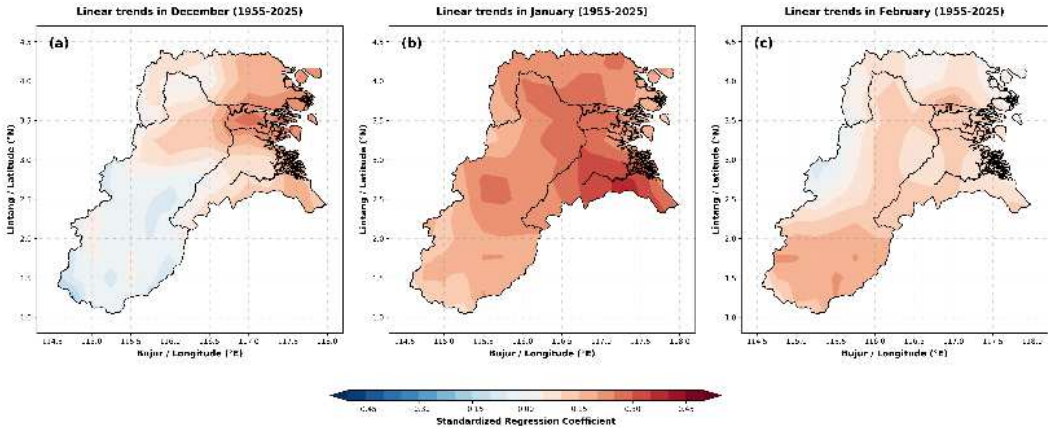


Figure 8. Spatial maps of standardized regression coefficients for linear monthly precipitation trends during December (a), January (b), and February (c) over North Kalimantan, 1955–2025. Blue (red) shading indicates positive (negative) trends. Only grid points significant at $\alpha = 0.05$ by the Mann–Kendall test are shown at full colour saturation; non-significant areas are lightened.

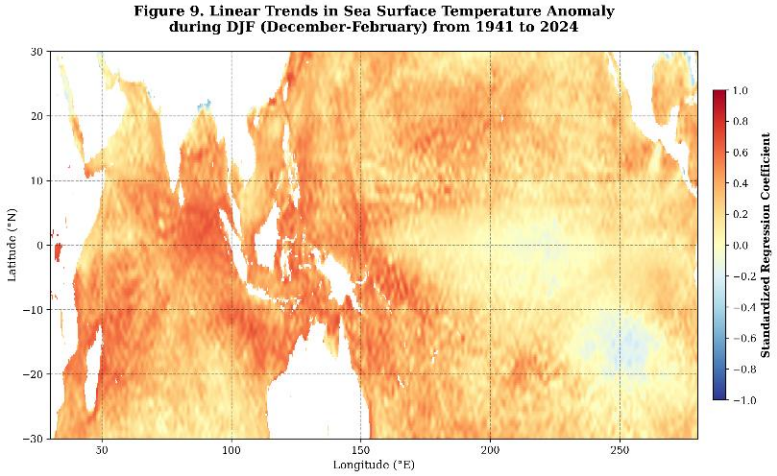


Figure 9. Global spatial map of standardized regression coefficients for linear DJF sea surface temperature anomaly (SSTa) trends, 1941–2024. Positive (negative) values indicate SST warming (cooling). Black stippling denotes statistical significance at $\alpha = 0.05$. The Sulawesi Sea and South China Sea,the primary moisture source regions for North Kalimantan,show among the most pronounced and statistically significant warming trends in the Indo-Pacific sector. *Note: The SST trend calculation utilizes the extended ERSSTv5 record starting from 1941 to comprehensively capture the multidecadal manifestation of the secular warming signal, providing a broader context for the primary 1955–2025 study period.*

4. Discussion

4.1 Disentangling Global versus Local Climate Controls

The four-mode Promax-rotated PCA decomposition presented in this study provides the most physically granular characterization of DJF precipitation variability in North Kalimantan to date. The results strongly suggest that rainfall variability over this compact equatorial province is organized into a strict hierarchy of forcing scales: from planetary (PC1: ENSO/IOD), through sub-regional synoptic (PC2: WPI/monsoon trough position), to purely mesoscale-local (PC3: Sulawesi Sea SST; PC4: orographic convection). This hierarchical architecture has important implications for seasonal prediction and attribution. Previous studies applied to broader Borneo or IMC domains using orthogonal Varimax rotation (e.g., Aldrian and Susanto, 2003; Juneng and Tangang, 2005) have identified one or two leading modes, typically associating them with ENSO and IOD. However, these orthogonal solutions mathematically suppress inter-mode correlations, potentially conflating locally driven patterns into residuals or folding them into spurious mixed-forcing modes

(Richman, 1986). The Promax approach adopted here releases this constraint, permitting PC3 and PC4 to emerge as statistically independent modes that share no teleconnection signature with any planetary-scale index. The implication is that a substantial fraction of Kaltara's DJF precipitation variability is fundamentally independent of the ENSO and IOD states, representing an inherent lower bound on the predictability of sub-regional precipitation over the IMC when relying solely on global forecast models.

4.2 Physical Mechanisms of the Locally Decoupled Modes

The physical mechanisms responsible for PC3 and PC4's independence from global teleconnections can be inferred with reasonable confidence from the spatial and atmospheric composite evidence. PC3's exclusive correlation with Sulawesi Sea and Makassar Strait SSTa (Figure 5c) and its associated mesoscale low-pressure anomaly over the eastern coastal waters (Figure 6, PC3 panel) indicate a thermally driven coastal convective mechanism. As the Sulawesi Sea warms,a process now proceeding at a statistically significant rate (Figure 9),the latent heat flux at the ocean–atmosphere interface increases, destabilizing the marine boundary layer and reducing convective inhibition. Under these conditions, diurnal coastal convergence and land–sea breeze circulations can trigger deep convection preferentially over the eastern coastal plain without requiring a large-scale monsoon enhancement. The progressive SST warming of the Sulawesi Sea since the mid-twentieth century (Figure 9) is highly consistent with why PC3 has become systematically more active after 2007, as the warm pool threshold for autonomous convective triggering is exceeded with increasing frequency.

PC4 presents a distinctly different mechanism: orographic forced lifting in the absence of a coherent large-scale flow anomaly. The anti-phase relationship between inland highland precipitation (positive) and offshore marine precipitation (negative) in the PC4 composite (Figure 3g,h) is a classic signature of orographic precipitation enhancement combined with rain-shadow suppression (Roe, 2005). The weak, spatially incoherent background wind field in the PC4 circulation composite (Figure 6, PC4 panel) suggests that this mode activates under ambient weak-gradient conditions. Under such low-wind conditions, differential thermal heating between the sun-exposed highland slopes and the adjacent cooler sea surface likely drives a mesoscale thermally direct circulation that channels boundary-layer moisture up the western mountain slopes.

These proposed mechanisms are dynamically supported by the thermodynamic and kinematic anomaly fields. For PC4, the isolated negative vertical velocity anomaly over the Crocker-Muller range at 850 hPa (Figure 6.1.a) aligns with localized forced ascent (ω < 0) initiating deep convection. For the coastal PC3 mode, the composite analysis reveals a localized low-pressure convergent anomaly (Figure 6) coupled with negative CAPE anomalies over the Sulawesi Sea (Figure 6.1.b). This thermodynamic signature is consistent with "CAPE consumption" (e.g., Ruppert et al., 2020), where continuous latent heat release over the eastern coastline during the active monsoon phase depletes the column's buoyant energy. Therefore, the empirical evidence strongly points to PC3 being a dynamically driven convective mode triggered by persistent low-level moisture convergence along the land-sea boundary, modulated autonomously by the secular warming of the Sulawesi Sea.

4.3 The 2007 Regime Shift in Its Indo-Pacific Context

The detection of a statistically significant regime shift in PC1 and PC3 at 2007 by the Pettitt test (Figure 7) is a key finding of this study. The year 2007 is particularly notable in the Indo-Pacific climate record: it marks a period of pronounced La Niña conditions (the strong 2007–2008 La Niña event), which may have provided the initial impetus for the observed step change in PC1 amplitude. However, a single ENSO event cannot explain a persistent upward shift persisting through 2025 an interpretation that requires a secular rather than episodic forcing. The global SST trend map (Figure 9) offers a compelling secular explanation: the Indo-Pacific warm pool region has experienced among the most rapid and statistically significant ocean warming globally since the 1940s (Bindoff et al., 2013; Lee et al., 2022). The progressive warming of the western Pacific thermodynamically amplifies Walker circulation anomalies during La Niña episodes (Cai et al., 2021), effectively intensifying the positive precipitation response over the IMC for the same ENSO forcing amplitude. For PC3, the post-2007 mean shift can be more directly attributed to the secular Sulawesi Sea warming (Figure 9), which has progressively lowered the thermodynamic threshold for autonomous coastal convective triggering (see Section 4.2). The co-occurrence of both shifts at 2007 is therefore likely not a single causal event but rather the temporal convergence of two independent secular warming trends crossing critical thermodynamic thresholds,a pattern consistent with nonlinear tipping-point behaviour documented in other tropical climate systems (Lenton et al., 2008).

The divergent within-season trend structure identified in Figure 8,intensifying December precipitation over the interior highlands, stationary January conditions, and a February drying trend along the eastern coast,adds important nuance to the regime shift narrative. This intra-seasonal pattern implies a lengthening and front-loading of the DJF wet season over the highland interior while the late-season coastal rainfall is simultaneously contracting. A physically plausible explanation is that the strengthened early-season moisture influx (consistent with amplified PC1 post-2007) front-loads convective activity over the orographically active interior, depleting tropospheric moisture reserves earlier in the monsoon season and leaving the eastern coast under a drier regime in February as the monsoon weakens and maritime SST gradients relax. This within-season structure has not been previously documented for North Kalimantan and merits further investigation with process-based modelling.

4.4 Practical and Policy Implications

The findings of this study carry direct implications for water resources management, agricultural planning, disaster risk reduction, and climate adaptation policy in North Kalimantan. The dominance of ENSO in driving PC1,which represents the largest mode of regional DJF precipitation variance,offers an encouraging foundation for seasonal prediction: ENSO state forecasts currently have skill at 6–9 month lead times (DelSole and Tippett, 2016), providing actionable seasonal outlooks for flood risk management in Kaltara's major river catchments (Sesayap, Kayan, and Sembakung). However, the complete independence of PC3 and PC4 from global indices implies that approximately 30–40% of DJF precipitation variability at the local scale cannot be captured by global seasonal prediction models. This intrinsically unpredictable component,driven by Sulawesi Sea thermal conditions and orographic convective dynamics,must be parameterised through high-resolution regional modelling to support sub-seasonal to seasonal (S2S) forecasting at the district level. The February drying trend along the eastern coast (Figure 8c) is particularly concerning for the urban populations of Tarakan and Nunukan, as a prolonged drying tendency threatens freshwater reservoir sustainability in the absence of compensating groundwater recharge. Climate adaptation strategies for coastal Kaltara should incorporate this divergent within-season trend into infrastructure planning horizons.

4.5 Limitations and Future Directions

Several limitations of this study should be acknowledged. First, while the ERA5 reanalysis was rigorously validated against the BMKG observational dataset, the *in-situ* network relies on seven aggregated Seasonal Zones (ZOM) representing a vast, topographically complex area of 72,567 km². This relatively sparse spatial density means that localized micro-climatic biases in the reanalysis, particularly over the remote Crocker-Muller highlands where physical gauges are virtually absent, cannot be entirely ruled out. Future work should incorporate denser sub-district gauge networks or high-resolution satellite retrievals (e.g., IMERG, CHIRPS) to further constrain orographic precipitation uncertainties. Second, the Pettitt test identifies the most likely location of a single abrupt change point; it cannot distinguish between a genuine step change and a monotonic trend that inflects at 2007. Application of multiple change-point detection algorithms,such as the CUSUM method or penalised regression approaches,would strengthen the robustness of the 2007 shift finding. Third, the physical mechanisms attributed to PC3 and PC4 are inferred from composite and correlation analysis; they require confirmation through high-resolution regional climate modelling or process-based mesoscale simulations that can explicitly resolve the Sulawesi Sea boundary layer convection and highland orographic forcing. Fourth, the study period extends backward to 1955 via ERA5 back-extension, for which assimilated observation density is lower than for the post-satellite era (post-1979); trend estimates prior to ~1979 carry larger uncertainty. Future studies should leverage ocean reanalysis products with higher spatial resolution,such as GLORYS12 or ORAS5,to more precisely characterise Sulawesi Sea SST variability and its coupling to PC3 precipitation variability at monthly and weekly timescales.

5. Conclusion

This study has produced the first 71-year (1955–2025) hierarchical decomposition of December–February (DJF) precipitation variability over North Kalimantan using Promax-oblique-rotated PCA applied to high-resolution ERA5 data. Four physically distinct and statistically robust modes of variability were identified, collectively revealing a multi-scale forcing architecture that orthogonal methods cannot resolve. PC1, the dominant regional mode, responds strongly to La Niña conditions and IOD negative-phase co-occurrence, affirming the primacy of global teleconnection control over large-scale DJF moisture enhancement. PC2 captures an

orographically mediated north–south precipitation gradient sensitive to the Western Pacific circulation, representing the sub-regional scale of the monsoon trough variability. Critically, PC3 and PC4 are demonstrated to be entirely independent of all tested global climate indices,governed instead by local Sulawesi Sea SST warming and mesoscale orographic convection, respectively,a finding that has direct consequences for seasonal prediction skill over the province.

The detection of a statistically significant regime shift at 2007 in the PC1 and PC3 modes by the non-parametric Pettitt test reveals that North Kalimantan's DJF precipitation system underwent an abrupt reorganisation approximately two decades ago, likely driven by the thermodynamic amplification of ENSO forcing and the progressive warming of the Sulawesi Sea warm pool. Simultaneously, a within-season divergence in precipitation trends has emerged: December rainfall intensifies over the western highland interior, January remains stationary, and February exhibits a significant drying tendency along the eastern coastal margin. Together, these findings constitute strong observational evidence for climate-driven restructuring of the monsoonal precipitation system over equatorial Borneo.

By demonstrating the hierarchical co-existence of globally forced and locally autonomous precipitation modes, this work underscores a fundamental limitation of both state-of-the-art global seasonal forecast models,which cannot capture local SST- and orography-driven variability,and of previous PCA studies that imposed artificial orthogonality. The methodological framework introduced here,Promax rotation over a 71-year ERA5 record,provides a replicable template for revisiting precipitation variability decompositions across other complex terrains of the Indonesian Maritime Continent and tropical island chains globally.

Author Declarations

- **Funding:** The authors declare that no funds, grants, or other support were received during the preparation of this manuscript.

- **Conflicts of interest/Competing interests:** The authors declare they have no financial interests or personal relationships that could have appeared to influence the work reported in this paper.

- **Ethics approval:** Not applicable. (This study does not involve human participants or animals).

- **Consent to participate:** Not applicable.
- **Consent for publication:** Not applicable.
- **Availability of data and material:** The ERA5 reanalysis data are available from the Copernicus Climate Change Service (C3S) Climate Data Store (https://cds.climate.copernicus.eu/). The ERSSTv5 and global climate indices are available from NOAA and JMA. The *in-situ* precipitation records are available upon reasonable request from BMKG (https://dataonline.bmkg.go.id/). Derived datasets are available from the corresponding author on reasonable request.
- **Code availability:** The code utilized for the Promax-rotated PCA, Pettitt test, and TFPW trend analysis relies on standard open-source Python libraries (scikit-learn, factor_analyzer, pyMannKendall). The specific analysis scripts are available from the corresponding author upon reasonable request.
- **Authors' contributions:** A. Mahardika conceptualized the study, performed the data acquisition, conducted the formal data analysis, prepared all figures and tables, and drafted the main manuscript text. A. Mulsandi supervised the research project, provided critical methodological guidance, validated the analytical framework, and substantially revised the manuscript. All authors read and approved the final manuscript.

References

Aldrian, E., & Susanto, R. D. (2003). Identification of three dominant rainfall regions within Indonesia and their relationship to sea surface temperature. International Journal of Climatology, 23(12), 1435–1452. https://doi.org/10.1002/joc.950

Ashok, K., Guan, Z., & Yamagata, T. (2003). Influence of the Indian Ocean Dipole on the Australian winter rainfall. Geophysical Research Letters, 30(15), 1821. https://doi.org/10.1029/2003GL017926

Bindoff, N. L., Stott, P. A., AchutaRao, K. M., Allen, M. R., Gillett, N., Gutzler, D., ... & Zhang, X. (2013). Detection and attribution of climate change: from global to regional. In T. F. Stocker et al. (Eds.), Climate Change 2013: The Physical Science Basis. Contribution of Working Group I to the Fifth Assessment Report of the IPCC. Cambridge University Press. https://doi.org/10.1017/CBO9781107415324.022

Bretherton, C. S., Widmann, M., Dymnikov, V. P., Wallace, J. M., & Bladé, I. (1999). The effective number of spatial degrees of freedom of a time-varying field. Journal of Climate, 12(7), 1990–2009. https://doi.org/10.1175/1520-0442(1999)012<1990:TENOSD>2.0.CO;2

Cai, W., Santoso, A., Collins, M., Dewitte, B., Karamperidou, C., Kug, J.-S., ... & McPhaden, M. J. (2021). Changing El Niño–Southern Oscillation in a warming climate. Nature Reviews Earth & Environment, 2(9), 628–644. https://doi.org/10.1038/s43017-021-00199-z

Chang, C.-P., Wang, Z., McBride, J., & Liu, C.-H. (2005). Annual cycle of Southeast Asia,Maritime Continent rainfall and the asymmetric monsoon transition. Journal of Climate, 18(2), 287–301. https://doi.org/10.1175/JCLI-3257.1

DelSole, T., & Tippett, M. K. (2016). Forecast comparison based on random walks. Monthly Weather Review, 144(2), 615–626. https://doi.org/10.1175/MWR-D-15-0218.1

Eschenbach, W. (2023). High-resolution orographic precipitation on Borneo: Climatic controls and hydrological implications. Journal of Hydrometeorology, 24(3), 411–428. https://doi.org/10.1175/JHM-D-22-0085.1

Hannachi, A., Jolliffe, I. T., & Stephenson, D. B. (2007). Empirical orthogonal functions and related techniques in atmospheric science: A review. International Journal of Climatology, 27(9), 1119–1152. https://doi.org/10.1002/joc.1499

Hendon, H. H. (2003). Indonesian rainfall variability: Impacts of ENSO and local air–sea interaction. Journal of Climate, 16(11), 1775–1790. https://doi.org/10.1175/1520-0442(2003)016<1775:IRVIOE>2.0.CO;2

Hersbach, H., Bell, B., Berrisford, P., Hirahara, S., Horányi, A., Muñoz-Sabater, J., ... & Thépaut, J.-N. (2020). The ERA5 global reanalysis. Quarterly Journal of the Royal Meteorological Society, 146(730), 1999–2049. https://doi.org/10.1002/qj.3803

Huang, B., Thorne, P. W., Banzon, V. F., Boyer, T., Chepurin, G., Lawrimore, J. H., ... & Zhang, H.-M. (2017). Extended Reconstructed Sea Surface Temperature, version 5 (ERSSTv5): Upgrades, validations, and intercomparisons. Journal of Climate, 30(20), 8179–8205. https://doi.org/10.1175/JCLI-D-16-0836.1

Juneng, L., & Tangang, F. T. (2005). Evolution of ENSO-related rainfall anomalies in Southeast Asia region and its relationship with atmosphere–ocean variations in Indo-Pacific sector. Climate Dynamics, 25(4), 337–350. https://doi.org/10.1007/s00382-005-0031-6

Kendall, M. G. (1975). Rank Correlation Methods (4th ed.). Charles Griffin.

Lee, S.-K., Lumpkin, R., Gomez, F., Yeager, S., Lopez, H., Takglis, F., ... & Dong, S. (2022). Human-induced changes in the global meridional overturning circulation are emerging from the Southern Ocean. Communications Earth & Environment, 3, 31. https://doi.org/10.1038/s43247-022-00361-9

Lenton, T. M., Held, H., Kriegler, E., Hall, J. W., Lucht, W., Rahmstorf, S., & Schellnhuber, H. J. (2008). Tipping elements in the Earth's climate system. Proceedings of the National Academy of Sciences, 105(6), 1786–1793. https://doi.org/10.1073/pnas.0705414105

Mann, H. B. (1945). Nonparametric tests against trend. Econometrica, 13(3), 245–259. https://doi.org/10.2307/1907187

Neale, R., & Slingo, J. (2003). The Maritime Continent and its role in the global climate: A GCM study. Journal of Climate, 16(5), 834–848. https://doi.org/10.1175/1520-0442(2003)016<0834:TMCAIR>2.0.CO;2

North, G. R., Bell, T. L., Cahalan, R. F., & Moeng, F. J. (1982). Sampling errors in the estimation of empirical orthogonal functions. Monthly Weather Review, 110(7), 699–706. https://doi.org/10.1175/1520-0493(1982)110<0699:SEITEO>2.0.CO;2

Pettitt, A. N. (1979). A non-parametric approach to the change-point problem. Applied Statistics, 28(2), 126–135. https://doi.org/10.2307/2346729

Qian, J.-H. (2008). Why precipitation is mostly concentrated over islands in the Maritime Continent. Journal of the Atmospheric Sciences, 65(4), 1428–1441. https://doi.org/10.1175/2007JAS2422.1

Ramage, C. S. (1968). Role of a tropical 'Maritime Continent' in the atmospheric circulation. Monthly Weather Review, 96(6), 365–370. https://doi.org/10.1175/1520-0493(1968)096<0365:ROATMC>2.0.CO;2

Richman, M. B. (1986). Rotation of principal components. Journal of Climatology, 6(3), 293–335. https://doi.org/10.1002/joc.3370060305

Roe, G. H. (2005). Orographic precipitation. Annual Review of Earth and Planetary Sciences, 33, 645–671. https://doi.org/10.1146/annurev.earth.33.092203.122541

Ruppert, J. H., Klocke, D., Bony, S., & Stevens, B. (2020). Diurnal circulation adjustment and organized deep convection. Journal of the Atmospheric Sciences, 77(9), 2807–2828. https://doi.org/10.1175/JAS-D-19-0167.1

Saji, N. H., Goswami, B. N., Vinayachandran, P. N., & Yamagata, T. (1999). A dipole mode in the tropical Indian Ocean. Nature, 401(6751), 360–363. https://doi.org/10.1038/43854

Saji, N. H., & Yamagata, T. (2003). Possible impacts of Indian Ocean Dipole mode events on global climate. Climate Research, 25(2), 151–169. https://doi.org/10.3354/cr025151

Tarek, M., Brissette, F. P., & Arsenault, R. (2020). Evaluation of the ERA5 reanalysis as a potential reference dataset for hydrological modelling over North America. Hydrology and Earth System Sciences, 24(5), 2527–2544. https://doi.org/10.5194/hess-24-2527-2020

Thurstone, L. L. (1947). Multiple Factor Analysis. University of Chicago Press.

Webster, P. J., Moore, A. M., Loschnigg, J. P., & Leben, R. R. (1999). Coupled ocean–atmosphere dynamics in the Indian Ocean during 1997–98. Nature, 401(6751), 356–360. https://doi.org/10.1038/43848